Sweet, sugar-coated hierarchical platinum nanostructures for easy support, heterogenization and separation

Dennis Woitassek [1,+], José G. Moya-Cancino [1,+], Yangyang Sun [1], Yefan Song [1], Dennis Woschko [1], Stefan Roitsch [2] and Christoph Janiak [1,*]

Keywords: ionic liquids; platinum; carbohydrates; hierarchical nanostructures; supported nanoparticles; hydrosilylation; sugar; saccharide

Table of Contents

Section

S1 Sources of chemicals

S2 Characterization of the ionic liquid 1-butyl-3-methylimidazoliumbis(trifluoromethylsulfonyl)imide ([BMIm]NTf_2)

S3 Synthesis parameters and analyses of sugar-coated platinum nanostructures (SC-Pt-NS) in 1-butyl-3-methylimidazoliumbis(trifluoromethylsulfonyl)imide ([BMIm]NTf2)

S4 Fourier-transform infrared (FTIR) spectroscopy measurements

S5 MALDI-TOF mass spectrometry

S6 Effect of water in the synthesis of platinum nanoparticles in IL

S7 Carbohydrate-free platinum nanoparticles synthesized in 1-butyl-3-methylimidazolium-bis(trifluoromethylsulfonyl)imide ([BMIm]NTf_2)

S8 Analysis of thermally treated sugars in IL

S9 Hydrosilylation activity and product analysis

S10 Gas chromatography (GC) analysis

S1 Sources of chemicals

Table S1 Sources for starting materials and solvents.

Items	Manufacturer
Hexachloridoplatinic acid hexahydrate ($H_2PtCl_6 \cdot 6H_2O$, Pt-38%)	TCI
Sucrose ($C_{12}H_{22}O_{11}$)	household sugar
D(-)-fructose ($C_6H_{12}O_6$, ≥ 99.5%)	Carl Roth
Acetonitrile (≥ 99.9%)	VWR Chemicals
Chloroform-d (99.8 atom % D)	Sigma-Aldrich
Phenylacetylene (97%)	Carbolution
Triethylsilane (99%)	Carbolution
1-Chlorobutane (≥ 99%)	Merck
1-Methylimidazole (99%)	Fluorochem
Lithium bis(trifluoromethanesulfonyl)imide (99%)	Fluorochem

S2 Characterization of the ionic liquid 1-butyl-3-methylimidazoliumbis(trifluoromethylsulfonyl)imide ([BMIm]NTf_2)

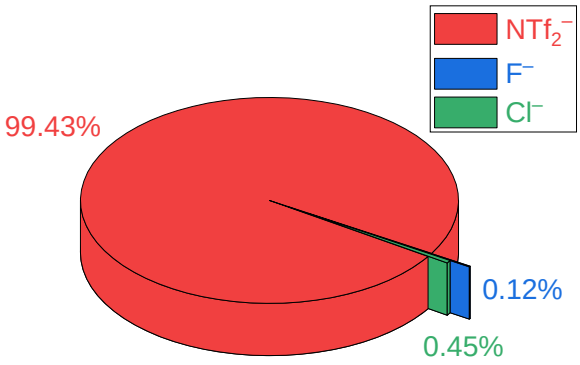

Figure S1 Ion chromatographic measurement (IC) of the synthesized ionic liquid (IL) [BMIm]NTf_2. Anion purity of NTf_2^- (red) was ascertained with the average of two measurements, resulting in a weight percentage of 99.43%.

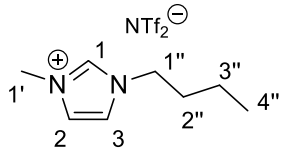

^{1}H NMR ($CDCl_3$, 300.13 MHz; internal standard = $CHCl_3$): δ 8.72 (s, 1H, 1-H), 7.31 (m, 2H, 2-3-H_2), 4.16 (t, 2H, ^3J = 7.5 Hz, 1''-H_2), 3.93 (s, 3H, 1'-H_3), 1.84 (tt, 2H, ^3J = 7.5 Hz, ^3J = 7.5 Hz 2''-H_2), 1.36 (qt, 2H, ^3J = 7.3 Hz, ^3J = 7.5 Hz, 3''-H_2), 0.95 (t, 3H, ^3J = 7.3 Hz, 4''-H_3).

^{13}C NMR ($CDCl_3$, 75.475 MHz; internal standard = $CHCl_3$): δ 136.2, 123.8, 122.4, 119.9 (q, ^1J = 321.1 Hz), 50.1, 36.4, 32.0, 19.5, 13.3.

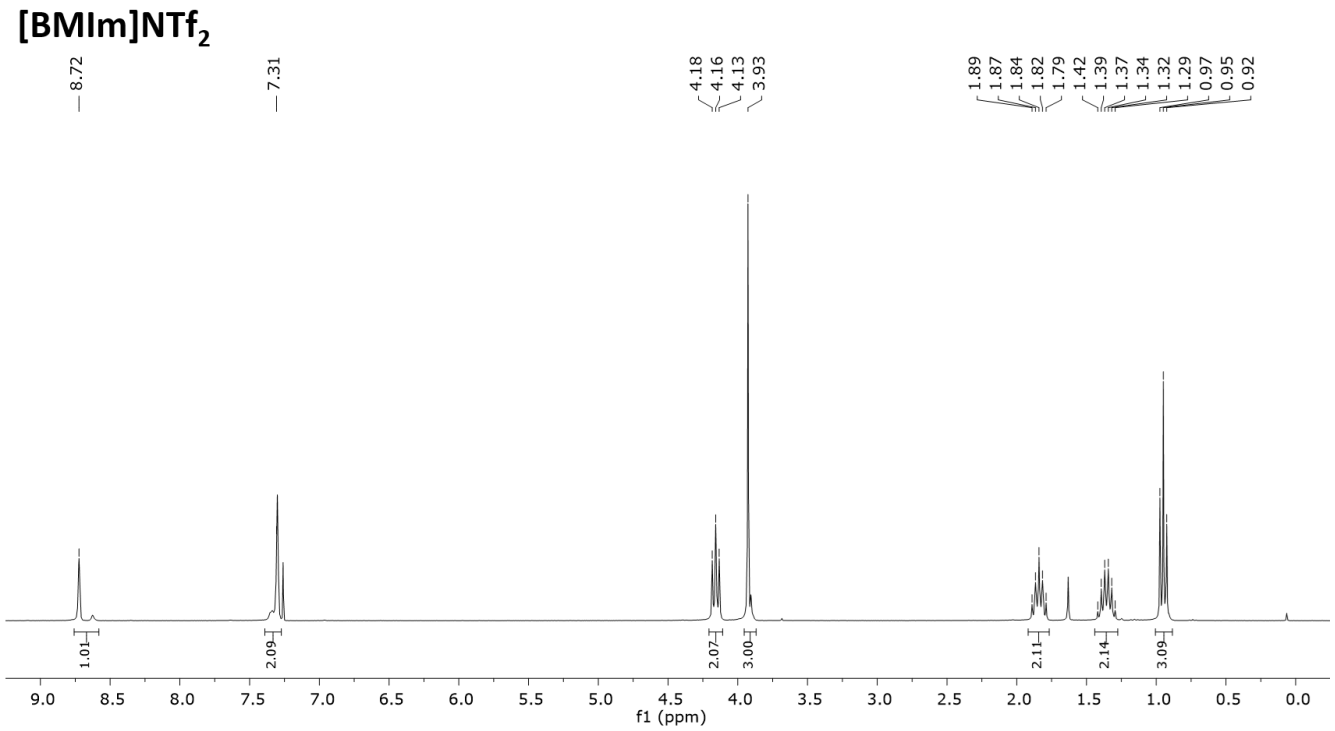

Figure S2 ^{1}H nuclear magnetic resonance (NMR) spectrum (300.13 MHz, $CDCl_3$) of [BMIm]NTf_2.

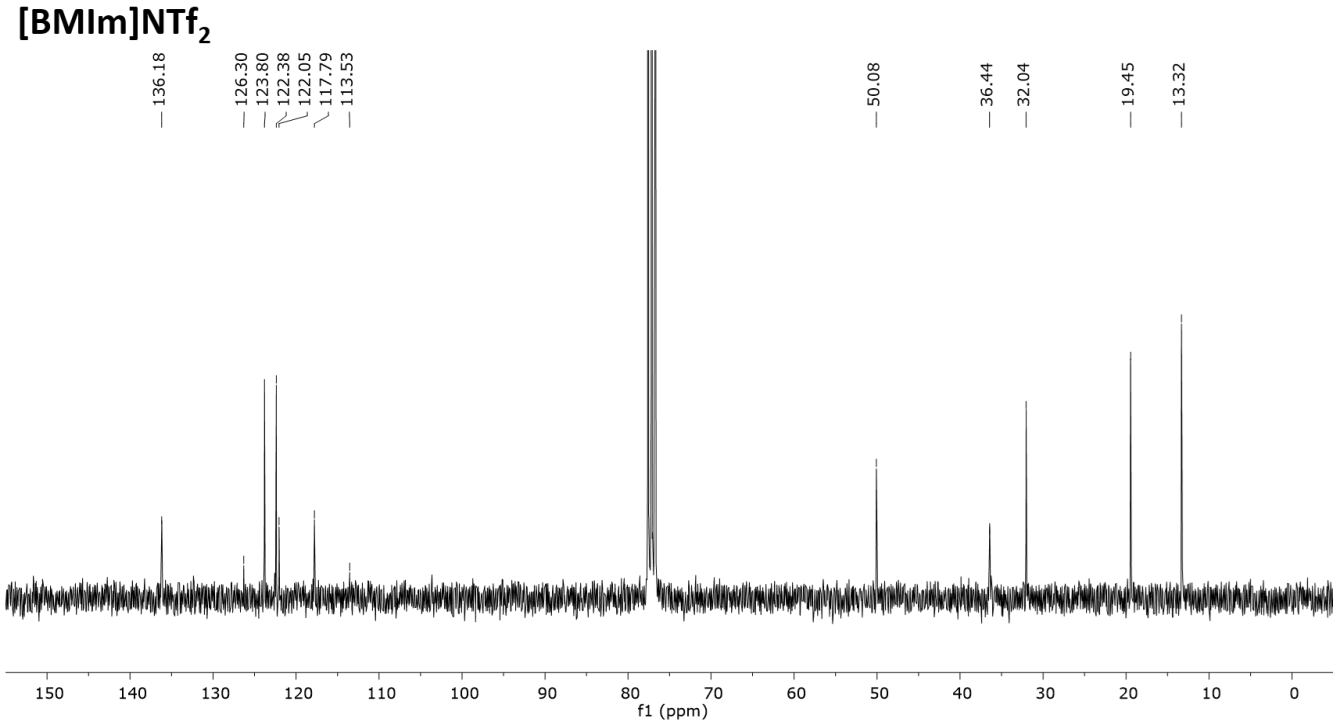

Figure S3 ^{13}C NMR spectrum ($CDCl_3$, 75.475 MHz) of [BMIm]NTf_2.

S3 Synthesis parameters and analyses of sugar-coated platinum nanostructures (SC-Pt-NS) in 1-butyl-3-methylimidazoliumbis(trifluoromethylsulfonyl)imide ([BMIm]NTf$_2$)

Table S2 Amount of reactants for sugar-coated Pt-nanostructures (SC-Pt-NS) in IL, Pt content and crystallite size of the product.

Sample [a]	Amount of $H_2PtCl_6 \cdot 6H_2O$	Sugar type	Amount of sugar	Amount of IL	theor. Pt wt.% [b]	Pt wt.% from AAS [c]	Average primary crystallite size (nm) [d]
S5	20.0 mg, 0.04 mmol	Sucrose	204.0 mg, 0.60 mmol	0.94 g	3.6 %	4.7 %	12 ± 1
S12	20.0 mg, 0.04 mmol	Sucrose	90.5 mg, 0.26 mmol	0.94 g	7.7 %	11.6 %	11 ± 1
S13	20.0 mg, 0.04 mmol	Sucrose	67.9 mg, 0.20 mmol	0.94 g	10.0 %	12.8 %	9 ± 1
S20	20.0 mg, 0.04 mmol	Sucrose	42.0 mg, 0.12 mmol	0.94 g	15.2 %	20.5 %	10 ± 1
S25	20.0 mg, 0.04 mmol	Sucrose	22.6 mg 0.07 mmol	0.94 g	25.0 %	24.7 %	8 ± 1
F6	20.0 mg, 0.04 mmol	D(-)-Fructose	214.0 mg, 1.18 mmol	0.94 g	3.4 %	5.7 %	11 ± 1
F10	20.0 mg, 0.04 mmol	D(-)-Fructose	95.2 mg, 0.53 mmol	0.94 g	7.3 %	10.1 %	10 ± 1
F14	20.0 mg, 0.04 mmol	D(-)-Fructose	71.5 mg, 0.40 mmol	0.94 g	9.5 %	13.6 %	11 ± 1
F17	20.0 mg, 0.04 mmol	D(-)-Fructose	44.2 mg, 0.24 mmol	0.94 g	14.6 %	16.9 %	10 ± 1
F32	20.0 mg, 0.04 mmol	D(-)-Fructose	23.8 mg, 0.13 mmol	0.94 g	24.0 %	31.5 %	10 ± 1

[a] Sample number is based on the rounded found Pt wt.% from AAS. The letter "S" and "F" indicate the used carbohydrate sucrose and fructose, respectively.

[b] Molar mass of $H_2PtCl_6 \cdot 6H_2O$ 517.90 g/mol with 37.67 wt.% Pt or 7.53 mg Pt from 20.0 mg of $H_2PtCl_6 \cdot 6H_2O$.

[c] Average of two measurements. The higher than theoretical value is due to partial dehydration of the carbohydrates together with some carbohydrate loss through the washing procedure.

[d] Average crystallite size and standard deviation are determined by applying the Scherrer equation (1) to the strongest reflexes ((111), (200), (220), (311)) observed in the respective sample:

$$L = K \times \lambda / (\Delta(2\theta) \times \cos \theta_0) \quad (1)$$

with L as average crystallite size, K as dimensionless shape factor, λ as wavelength, $\Delta(2\theta)$ as full width at half maximum (FWHM) in radians and θ as Bragg angle.

S3.1 Elemental analysis

CHNS elemental analysis of the IL-treated samples show the presence of sulfur and nitrogen as evidence of remaining IL traces. Based on the N and S percentage the IL content was estimated. The N to the S percentage in relation to the calculated ratio was close to the expected value for the fructose samples (0.9-1.0) and slightly higher for the sucrose samples (1.24-1.29). This higher N:S ratio is due to acetonitrile traces which remain enclosed (clathrated) in the caramelized sugars during the process of drying for 1 h.

Table S3 CHNS elemental analysis of sucrose, D(-)fructose, their thermally treated samples (S_{sup}, F_{sup}) and SC-Pt-NS samples.

Sample	C (%) (theor)	H (%) (theor)	O (%) (theor.)	N (%)	S (%)	IL-content (%)[a]
Sucrose[b]	42.20	6.53	-	-	-	-
	(42.11)	(6.48)	(51.41)			
D(-)-fructose[c]	39.88	6.86	-	-	-	-
	(40.00)	(6.71)	(53.28)			
S_{sup}	48.07	5.39		0.57	0.88	5.8
F_{sup}	48.37	5.46		0.57	0.76	5.0
S13	53.48	3.71		0.90	1.10	7.2
S25	45.55	3.47		0.56	0.66	4.3
F14	48.74	3.41		0.92	1.55	10.1
F32	38.60	2.71		1.31	1.96	12.8

[a] IL-content was calculated from the sulfur percentage based on the ratio of molar mass of IL (419.36 g mol^{-1}) to expected molar mass of sulfur in IL (2 S-atoms, 64.12 g mol^{-1}).

[b] $C_{12}H_{22}O_{11}$ (M = 342.30 g mol^{-1}).

[c] $C_6H_{12}O_6$ (M = 180.16 g mol^{-1}).

S3.2 Powder X-ray diffractometry (PXRD)

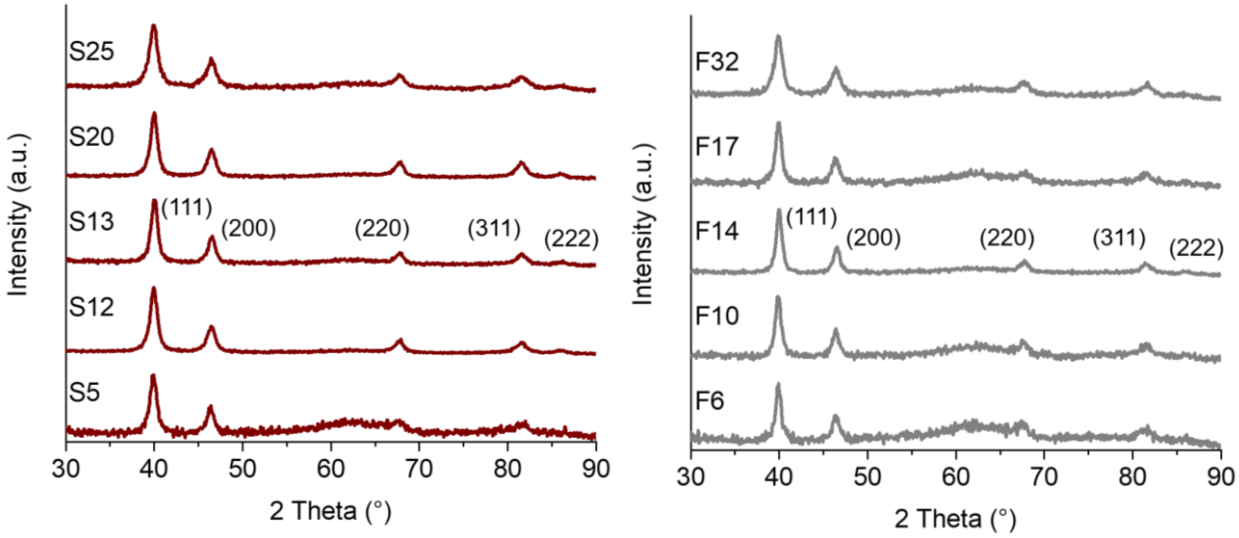

Figure S4 PXRD patterns of SC-Pt-NS (left: with sucrose; right: with fructose). In each pattern, the Pt metal reflections (111), (200), (220), (311) and (222) are visible, cf. simulation in Figure. 1 in the main text.

S3.3 Transmission electron microscopy (TEM)

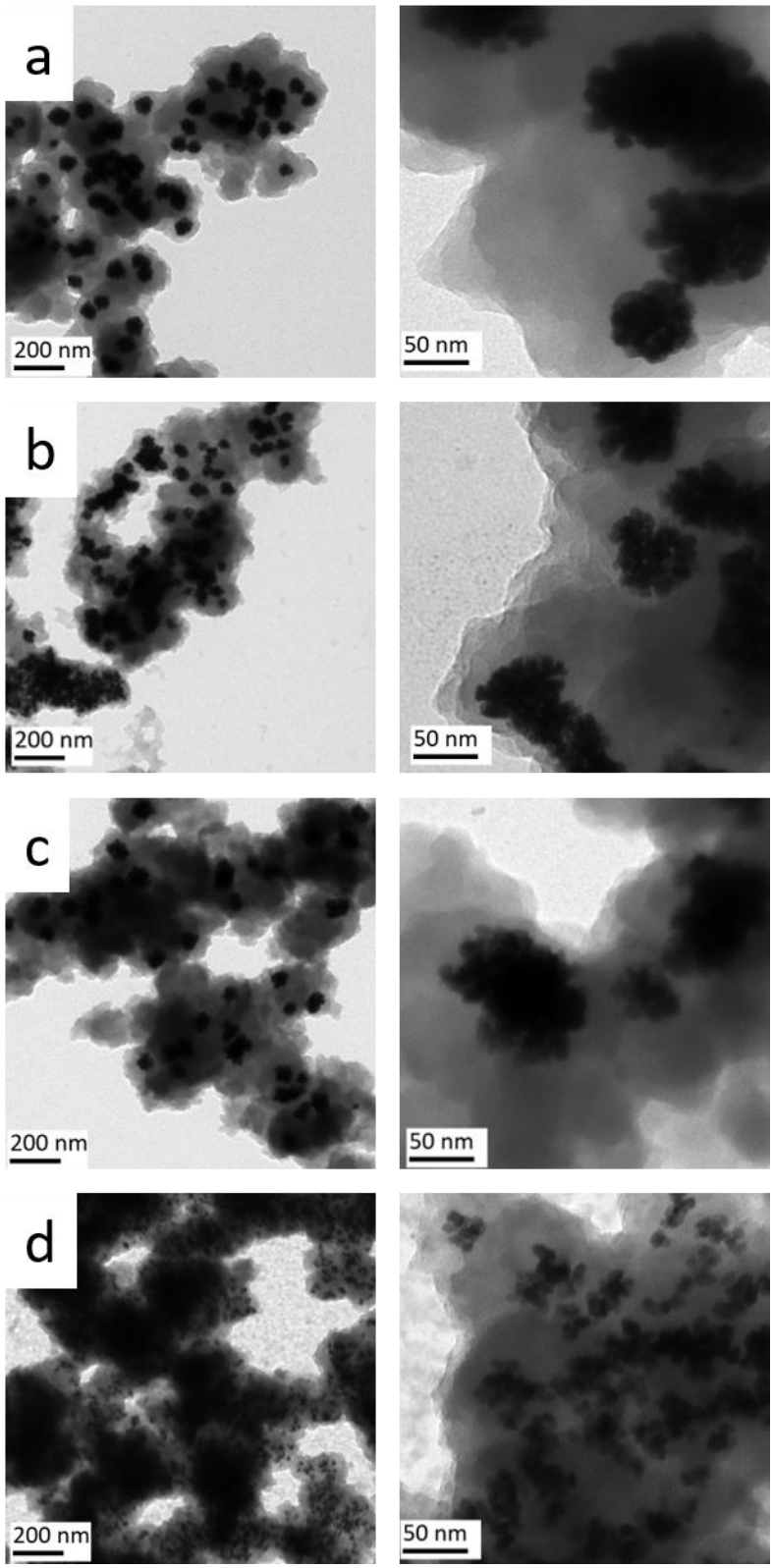

Figure S5 TEM images for samples after 1 year of storage. (**a**) S13, (**b**) S25, (**c**) F14 and (**d**) F32.

S3.4 Dynamic light scattering (DLS)

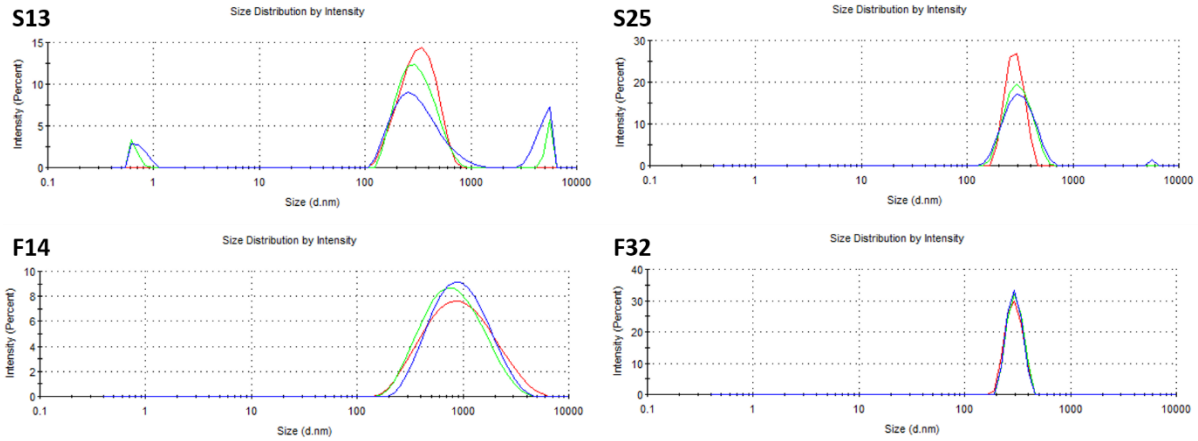

Figure S6 Dynamic light scattering (DLS) of SC-Pt-NS S13, S25, F14 and F32 with an average size of 330 nm, 300 nm, 1060 nm and 300 nm, respectively. Three measurements with automatically decided number of runs were done for each sample and are shown in different colors.

S4 Fourier-transform infrared (FTIR) spectroscopy measurements

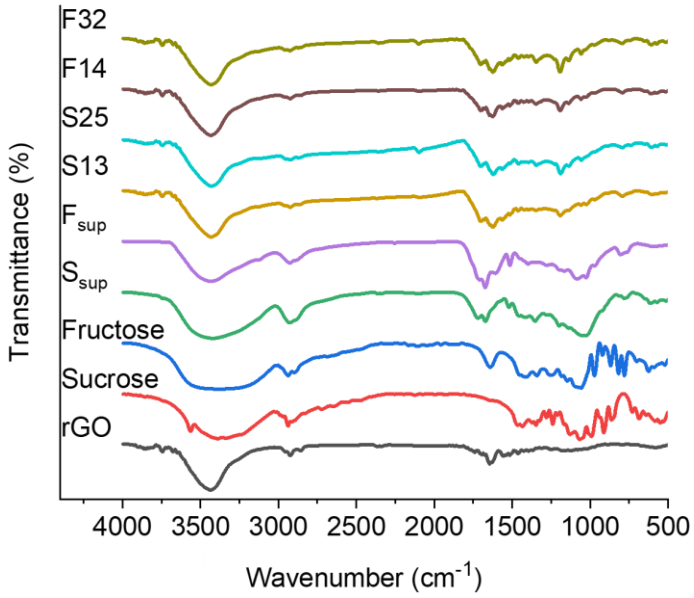

Figure S7 FTIR spectra of the samples S13, S25, F14 and F32 as KBr pellets. In addition, reference samples of sucrose, D(-)fructose, their respectively thermally treated samples (S_{sup}, F_{sup}) and reduced graphene oxide (rGO) are shown. The O-H peak at ~3400 cm^{-1} is due to the uptake of water by KBr during the sample preparation and overlaps with sample signals.

The obtained FTIR spectra of the reference samples fit to Max and Chapados [70]. From the analysis of the data, it is possible that during the synthesis the sugar partially decomposed, possibly under condensation, by observing the absence and reduction of the C-H and C-OH frequencies, respectively, and the presence of the H_2O small stretching frequency at ~2100 cm^{-1}. The coating retains functional groups, e.g. at ~1050 cm^{-1} and ~1350 cm^{-1}.

Table S4 FTIR frequencies identified for the SC-Pt-NS, which differ to the pure carbohydrates [70].

cm^{-1}	Type of vibration
~1050	C-O-C Stretching, C-O-H Stretching
~1140	C-O-C Stretching, C-O-C Bending
~1190	C-O-C Bending,
~1350	C-O-H Bending, H-C-H Bending
~1620	C=C Stretching
~1700	C=C Stretching
~2100	H_2O Stretching

S5 MALDI-TOF mass spectrometry

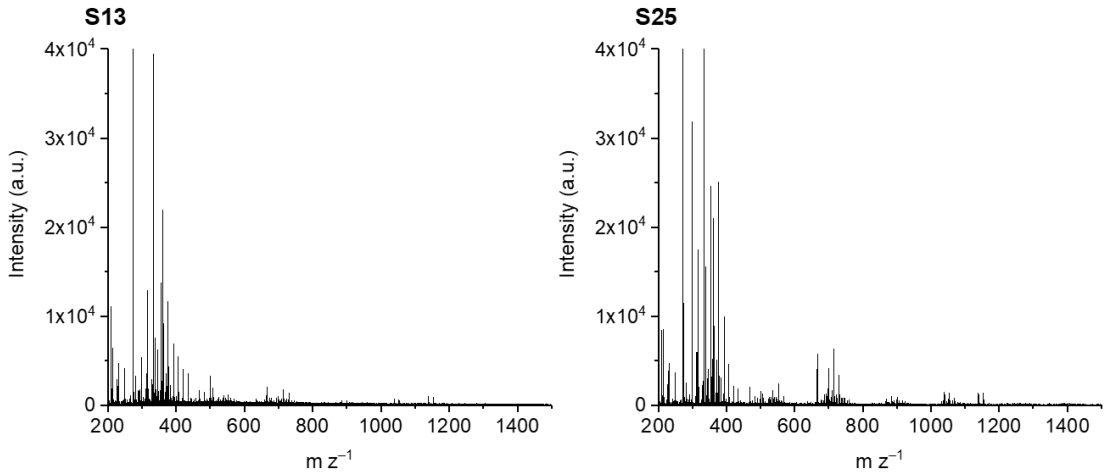

Figure S8 MALDI-TOF mass spectra of the SC-Pt-NS S13 and S25 from the matrix DHB.

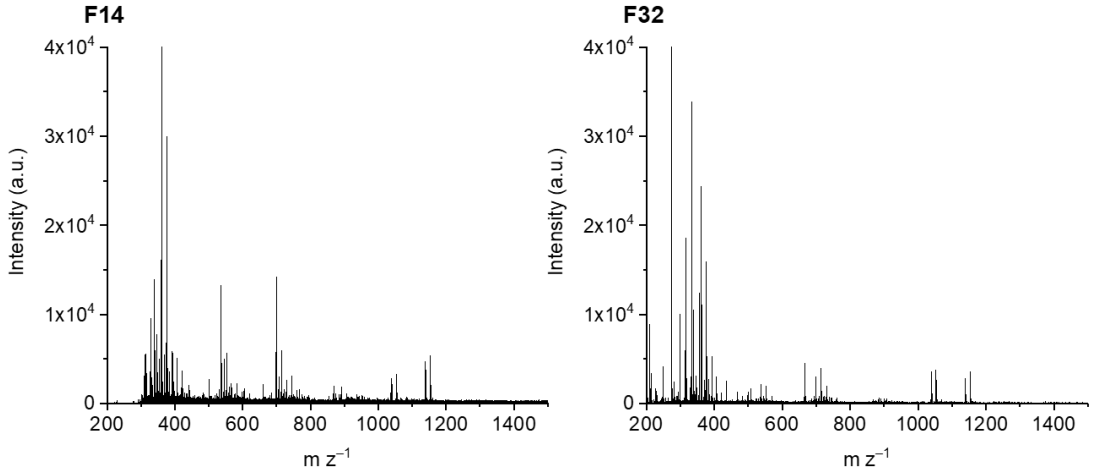

Figure S9 MALDI-TOF mass spectra of the SC-Pt-NS F14 and F32 from the matrix DHB.

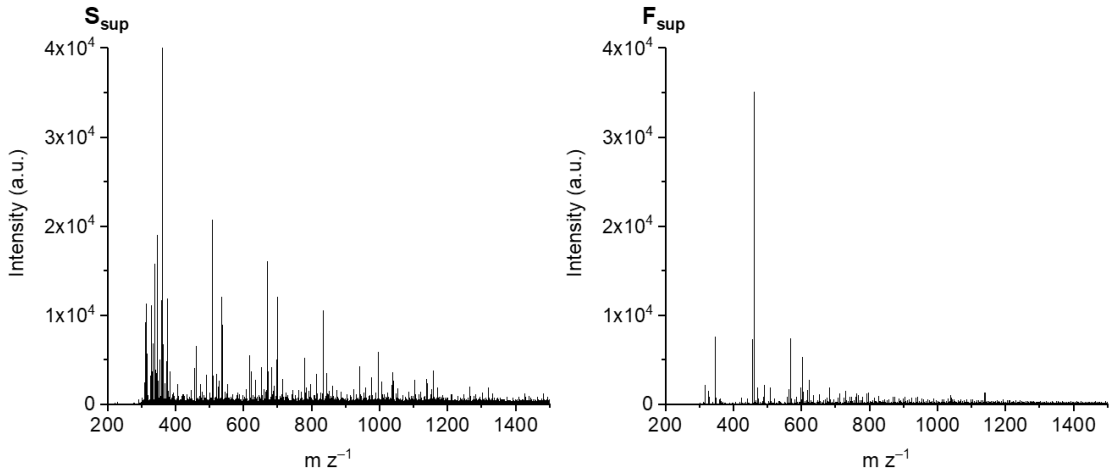

Figure S10 MALDI-TOF mass spectra of the saccharides S_{sup} and F_{sup} from the matrix DHB.

S6 Effect of water in the synthesis of platinum nanoparticles in IL

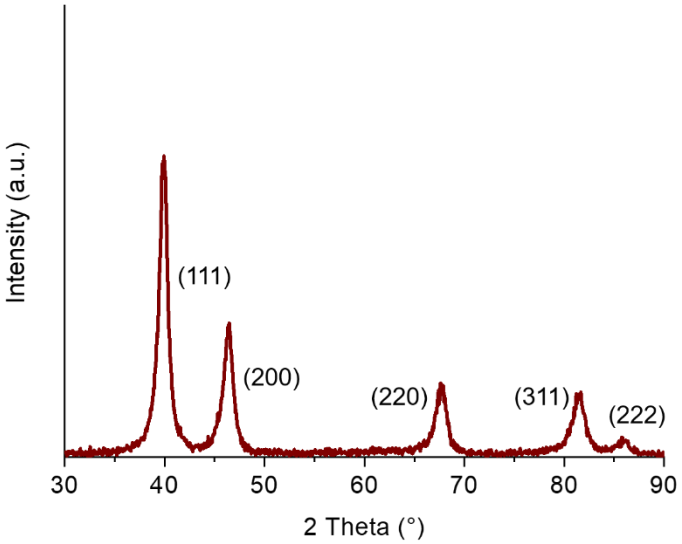

Figure S11 PXRD pattern of Pt-NPs synthesized in [BMIm]NTf_2 and water (5 wt.%). The reflections (111), (200), (220), (311) and (222) match the pattern for fcc-Pt metal (cf. Fig. 1 in the main text). By applying the Scherrer equation to the PXRD data, an average crystal size of ~8 nm was estimated.

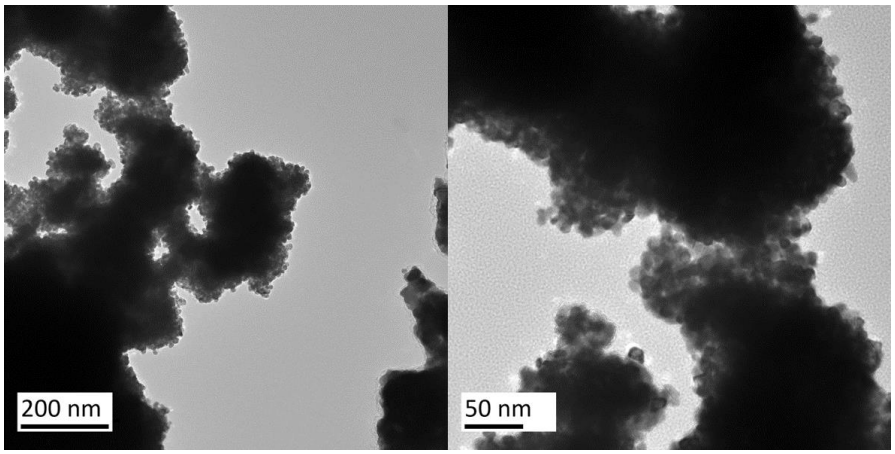

Figure S12 TEM images of Pt-NPs synthesized in [BMIm]NTf_2 and water (5 wt.%).

From the analysis we conclude that the water-content alone cannot be responsible to obtain the aggregated features observed in the SC-Pt-NS. Hence, the water formed upon partial decomposition (condensation) of the sugar molecules only plays a minor role in the formation of the sugar-coated nanostructures.

S7 Carbohydrate-free platinum nanoparticles synthesized in 1-butyl-3-methylimidazolium-bis(trifluoromethylsulfonyl)imide ([BMIm]NTf_2)

For comparison purposes, unsupported Pt-NPs were synthesized following the identical experimental steps but without the presence of a carbohydrate:

The Pt precursor $H_2PtCl_6 \cdot 6H_2O$ (20.0 mg, 0.04 mmol) was added to 0.94 g (0.65 mL) of the IL [BMIm]NTf_2. The mixture was stirred for 2 h at 400 rpm, followed by microwave heating for 10 min at 200 °C under 20 W microwave power. By addition of 3 mL of acetonitrile and centrifugation at 4000 rpm for 10 min a solid product was separated from the brown solution. The washing process using acetonitrile was repeated several times until after six washing cycles with a total of 18 mL of acetonitrile, a colorless solution was obtained. Finally, the solid product was dried at room temperature in an oil pump vacuum.

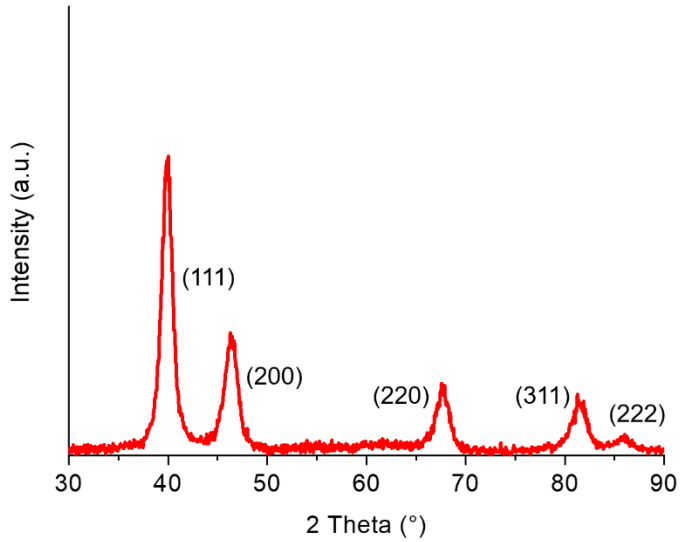

Figure S13 PXRD patterns of Pt-NPs synthesized in the IL [BMIm]NTf_2. The reflections (111), (200), (220), (311) and (222) match the pattern for fcc-Pt metal (cf. Fig. 1 in the main text).

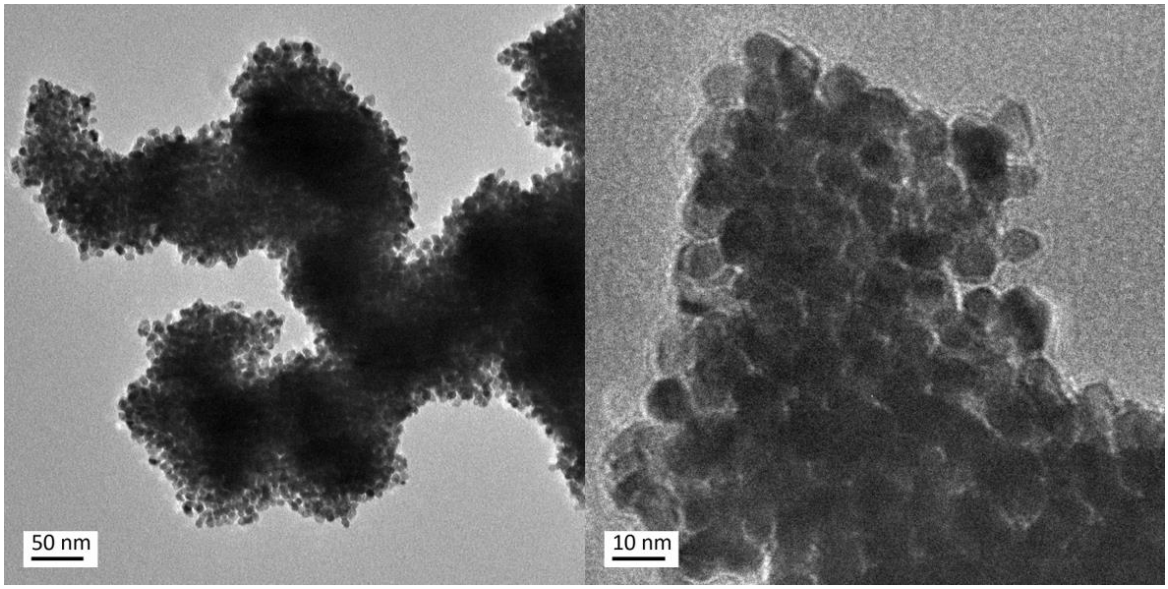

Figure S14 TEM images of agglomerated Pt-NPs synthesized in IL without the presence of sugars.

S8 Analysis of thermally treated sugars in IL

The sugars sucrose and D(–)-fructose were thermally treated in IL (in the absence of the Pt precursor) to analyze the changes incurred to the carbohydrates. The thermally treated sucrose and D(–)-fructose samples are labelled S_{sup} and F_{sup}, respectively.

The CHNS elemental analysis of S_{sup} and F_{sup} is given in Table S3.

The FTIR spectra of S_{sup} and F_{sup} are given in Figure S7.

S8.1 Powder X-ray diffractometry (PXRD)

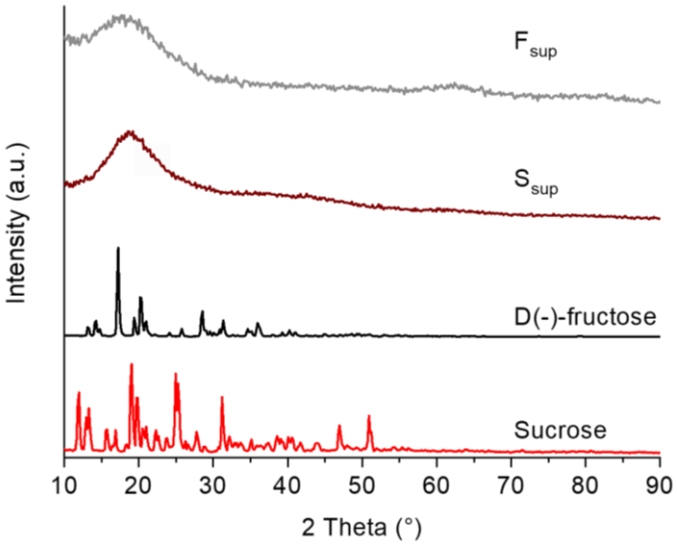

Figure S15 PXRD patterns of thermally treated sucrose and D(–)-fructose in the IL [BMIm]NTf_2 at the same conditions as in the synthesis of SC-Pt-NS (200 °C for 10 min microwave induced heating).

S8.2 Thermogravimetry analysis (TGA)

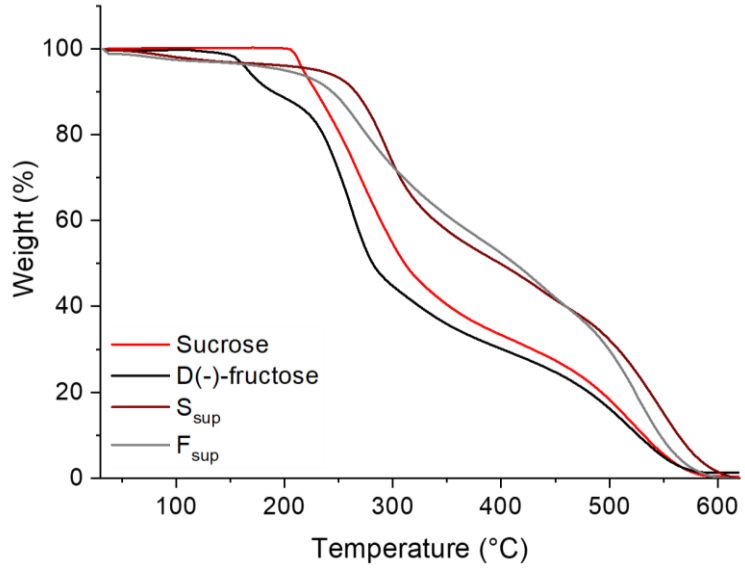

Figure S16 Thermogravimetric analysis (TGA) of neat sucrose and D(-)-fructose and of thermally treated sucrose and D(–)-fructose in the IL [BMIm]NTf_2 (200 °C for 10 min microwave induced heating). TGA at a heating rate of 5 °C min^{-1} under synthetic air.

S8.3 NMR spectroscopy

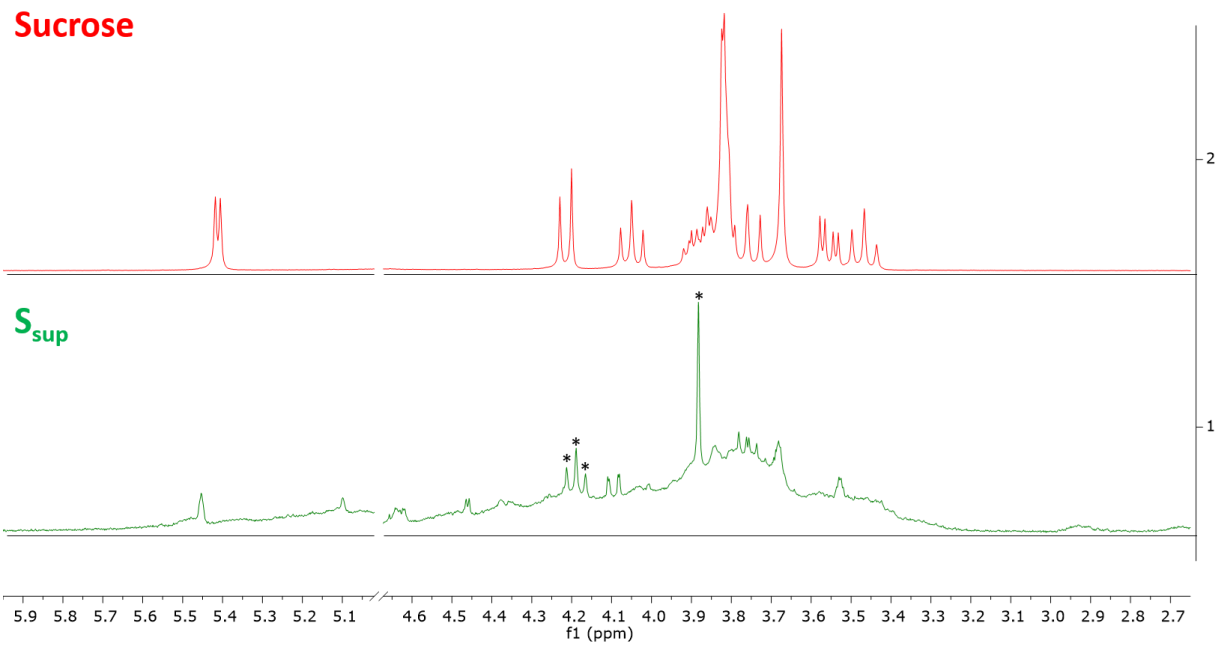

Figure S17 ^{1}H NMR spectra (D_2O, 300.13 MHz) of sucrose before (top) and after (bottom) thermal treatment in IL (S_{sup}, 200 °C for 10 min microwave induced heating). The region with the deuterated solvent (D_2O) signal at 4.79 ppm has been left out for clarity. In the spectrum of S_{sup}, a significant broadening of the baseline can be observed in the range from 3.1 to 5.5 ppm, possibly due to an inhomogeneous degradation of the carbohydrate. Furthermore, in the S_{sup} spectrum residual IL peaks are visible (signals marked with *).

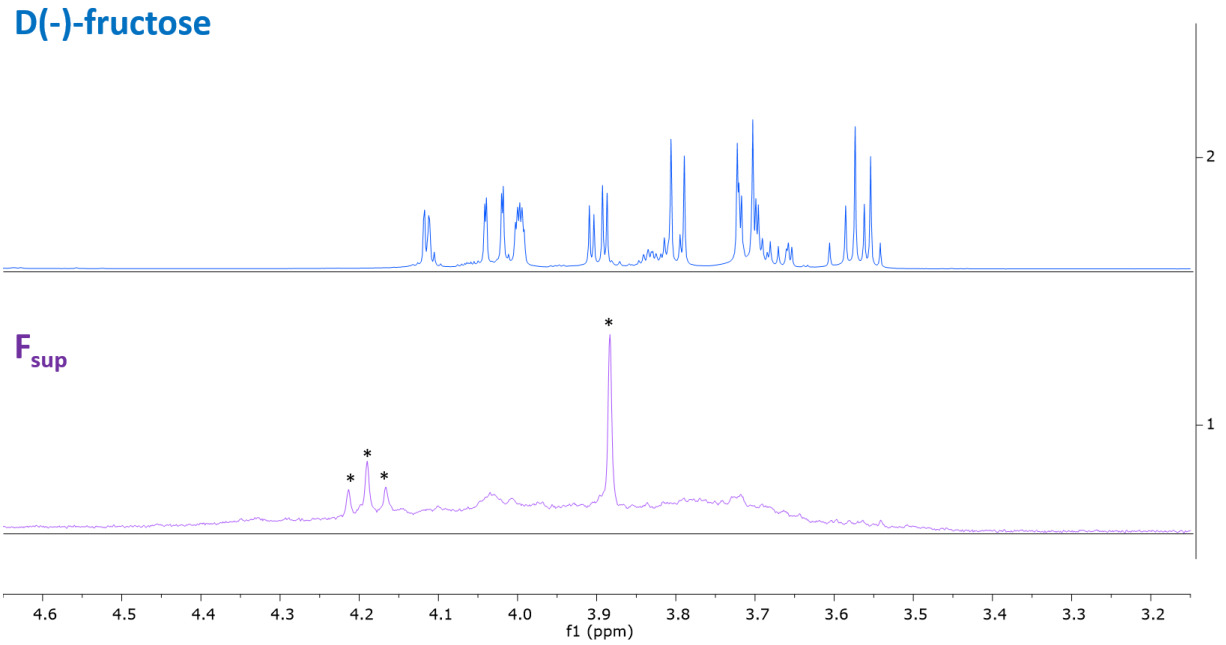

Figure S18 ^{1}H NMR spectra (D_2O, 300.13 MHz) of D(-)-fructose before (top) and after (bottom) thermal treatment in IL (F_{sup}, , 200 °C for 10 min microwave induced heating). In the spectrum of F_{sup}, a significant broadening can be observed in the range from 3.4 to 4.3 ppm, possibly due to an inhomogeneous degradation of the carbohydrate. Furthermore, in the F_{sup} spectrum residual IL signals are visible (signals marked with *).

S8.4 Gel permeation chromatography / size exclusion chromatography

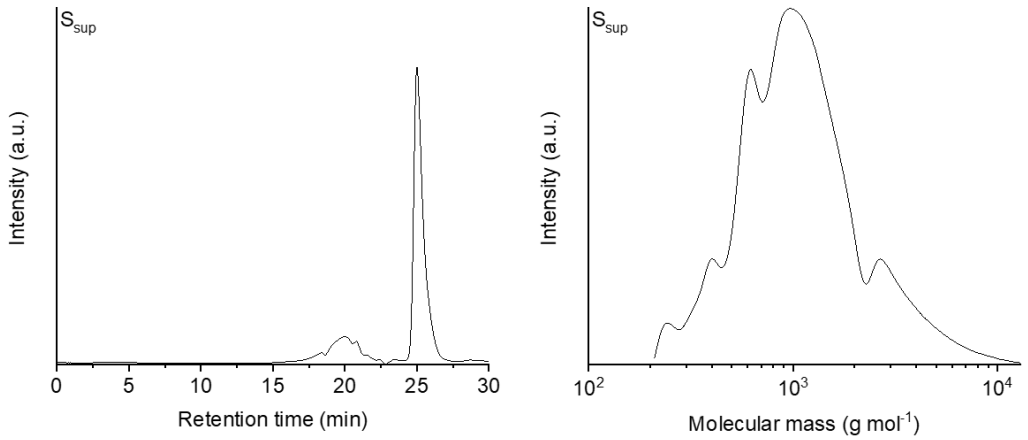

Figure S19 GPC/SEC measurements of thermally treated sucrose. The GPC chromatograms are shown on the left and the molecular mass distribution on the right side (retention time between 15 to 23 min). The sharp signal with a retention time of ~26 min is the internal standard.

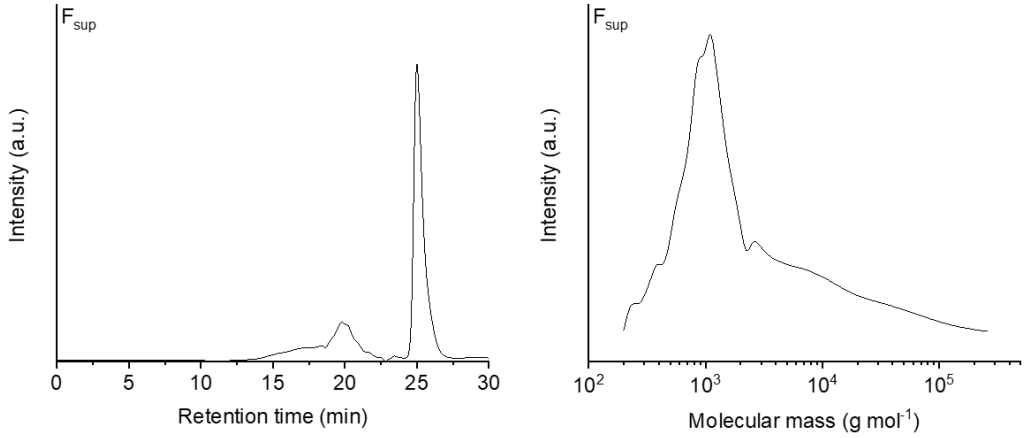

Figure S20 GPC/SEC measurements of thermally treated D-(-)-fructose. The GPC chromatograms are shown on the left and the molecular mass distribution on the right side (retention time between 12 to 23 min). The sharp signal with a retention time of ~26 min is the internal standard.

S9 Hydrosilylation activity and product analysis

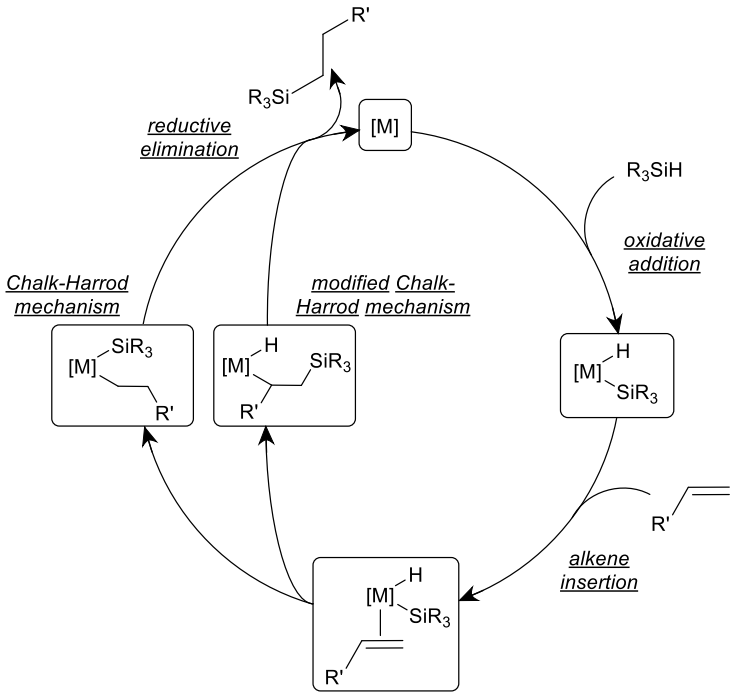

Figure S21 Chalk-Harrod Mechanism and a modified Chalk-Harrod mechanism for the transition metal catalysed hydrosilylation of alkenes [42,49].

Table S5 Activity of SC-Pt-NS samples in the hydrosilylation of phenylacetylene with triethylsilane.

Sample	mol Pt in SC-Pt-NS [a] (μmol)	Molar ratio substrate/Pt	Conversion (%)	Molar ratio distal/proximal from NMR [b]	Molar ratio distal/proximal from GC [c]
$H_2PtCl_6 \cdot 6H_2O$	2.26	2200	98	1.9	1.3
Pt-NP	4.60	1100	91	1.9	1.6
S5	0.14	35500	23	3.1	3.2
S12	0.31	15700	85	1.6	1.7
S13	0.66	7500	97	2.1	2.1
S20	0.60	8100	76	2.0	2.0
S25	1.28	3800	99	1.4	1.3
F6	0.15	32000	10	3.3	4.0
F10	0.29	17100	32	3.0	3.4
F14	0.72	6900	98	1.7	1.6
F17	0.46	10600	78	2.4	2.4
F32	0.86	3500	99	1.4	1.3

[a] General conditions: 4.9 mmol phenylacetylene and triethylsilane, time 5 min, microwave induced heating at 200 W, temperature 200 °C. For the samples presented in the main document (S13, S25, F14, F32 and the references $H_2PtCl_6 \cdot 6H_2O$ and Pt-NP) 1 mg were used, while for the other samples 0.5 mg of SC-Pt-NS were utilized. Molar values were calculated with the weigh-ins and the AAS analysis of SC-Pt-NS. Pt-content of $H_2PtCl_6 \cdot 6H_2O$ and Pt-NP were calculated in correlation to the molar weight and assuming pure Pt-NP, respectively.

[b] Determined by ^{1}H-NMR spectra from the solution after the reaction. Reference signals for the distal and proximal product were taken from the literature [71].

[c] Determined from peak areas.

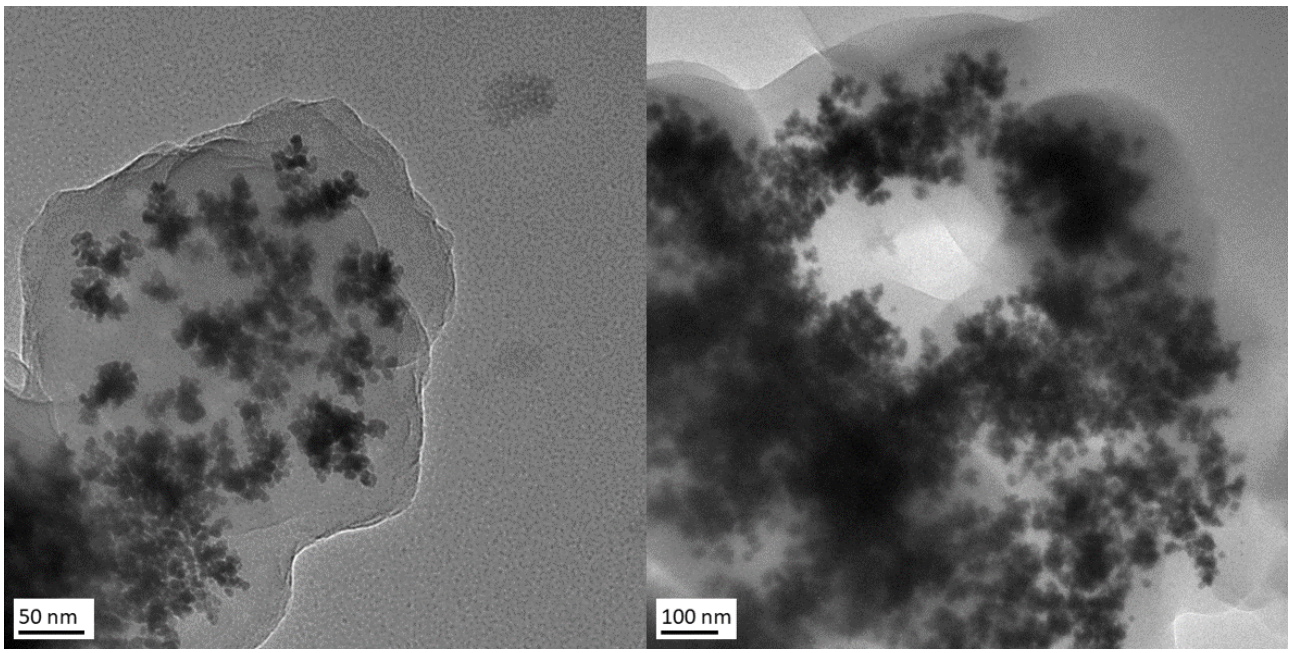

Figure S22 TEM-images of sample S25 after it was used for three consecutive hydrosilylation runs.

NMR analysis

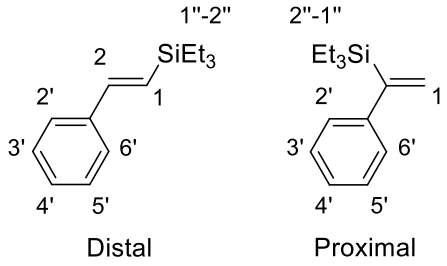

Distal:

^{1}H NMR ($CDCl_3$, 300.13 MHz; internal standard = TMS): δ 7.00 - 7.40 (m, 5H, 2′-6′-H_5), 6.81 (d, 1H, ^{3}J = 19.3 Hz, 2-H), 6.33 (d, 1H, ^{3}J = 19.3 Hz, 1-H), 0.75 – 1.00 (m, 9H, 3·2′′-H_3), 0.50 - 0.65 (m, 6H, 3·1′′-H_2).

^{13}C NMR ($CDCl_3$, 75.475 MHz; internal standard = $CHCl_3$): δ 145.0, 138.7, 128.6, 128.0, 126.5, 126.1, 7.6, 3.7.

Proximal:

^{1}H NMR ($CDCl_3$, 300.13 MHz; internal standard = TMS): δ 7.00 - 7.40 (m, 5H, 2′-6′-H_5), 5.77 (d, 1H, ^{3}J = 3.1 Hz, 1-H)*, 5.48 (d, 1H, ^{3}J = 3.1 Hz, 1-H)*, 0.75 – 1.00 (m, 9H, 3·2′′-H_3), 0.50 - 0.65 (m, 6H, 3·1′′-H_2); *signal assignment interchangeable [63].

^{13}C NMR ($CDCl_3$, 75.475 MHz; internal standard = $CHCl_3$): δ 150.6, 145.7, 128.9, 128.2, 126.8, 126.2, 7.4, 3.5.

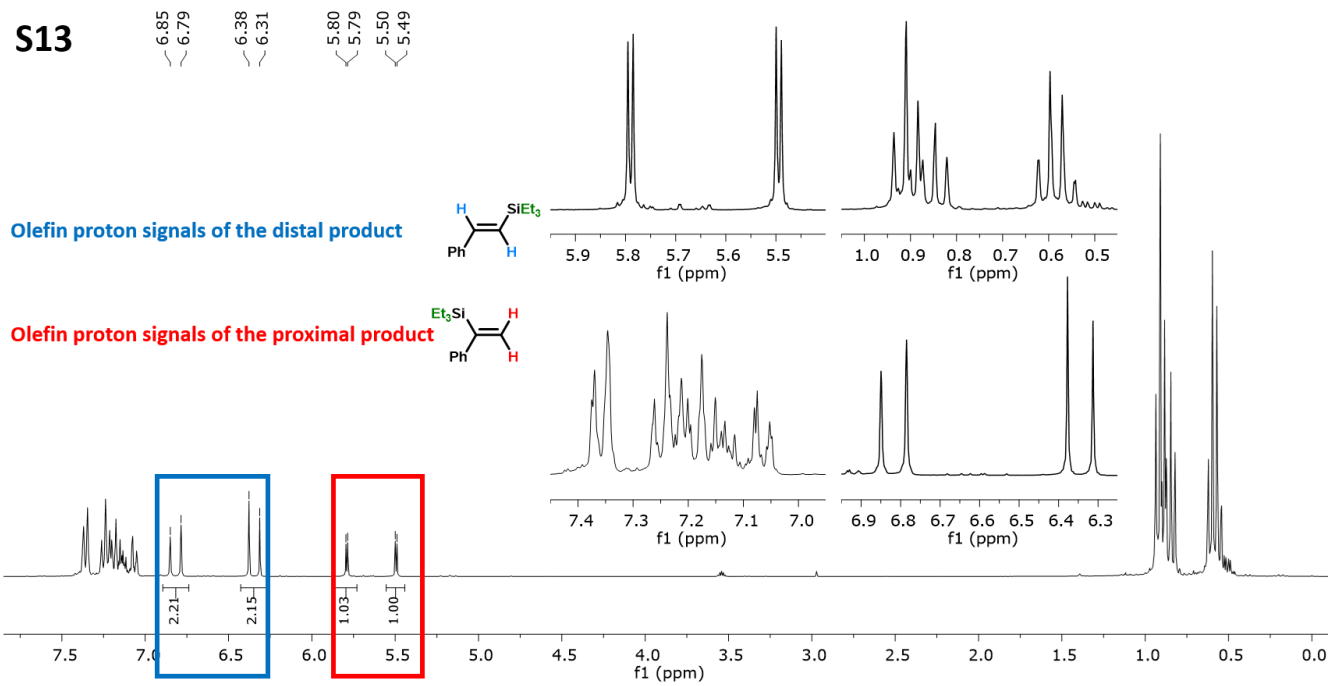

Figure S23 ^{1}H NMR spectrum (300.13 MHz, $CDCl_3$) with expanded sections of the hydrosilylation product from sample S13. The conversion was 98% and the molar distal/proximal ratio 2.1.

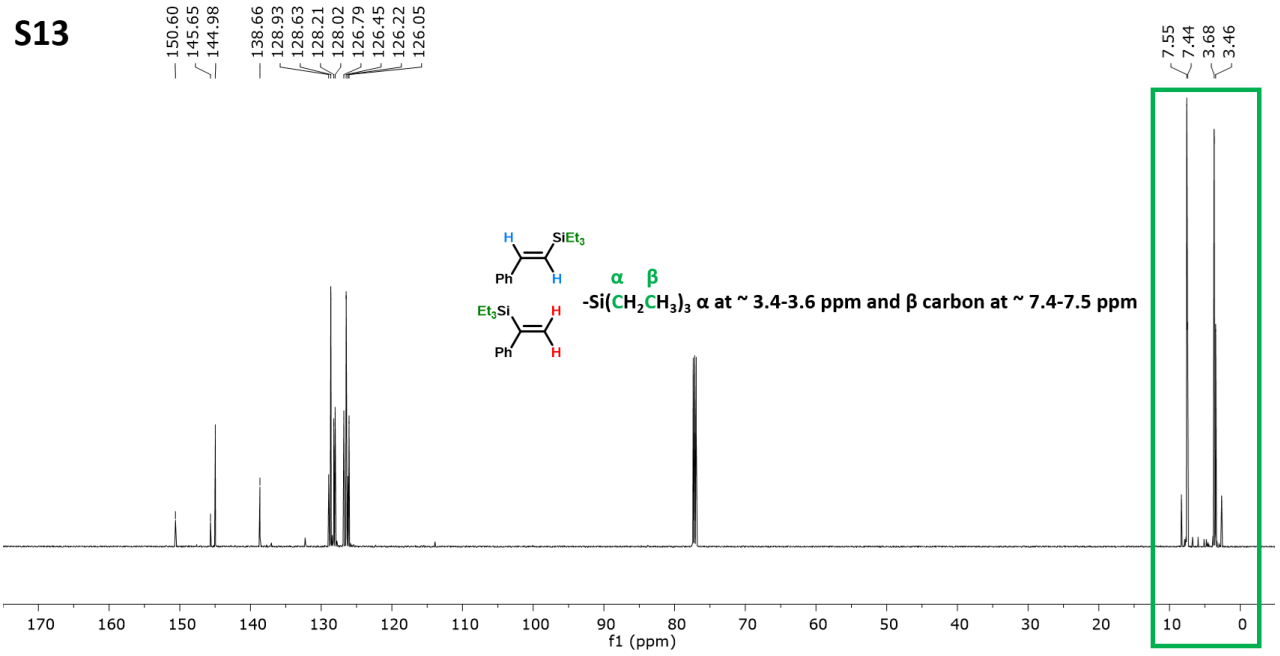

Figure S24 ^{13}C NMR spectrum (75.475 MHz, $CDCl_3$) of the hydrosilylation product from sample S13. Carbon α at ~3.4-3.6 ppm and carbon β at ~7.4-7.5 ppm. The two peaks each for α and β are due to the distal and proximal products.

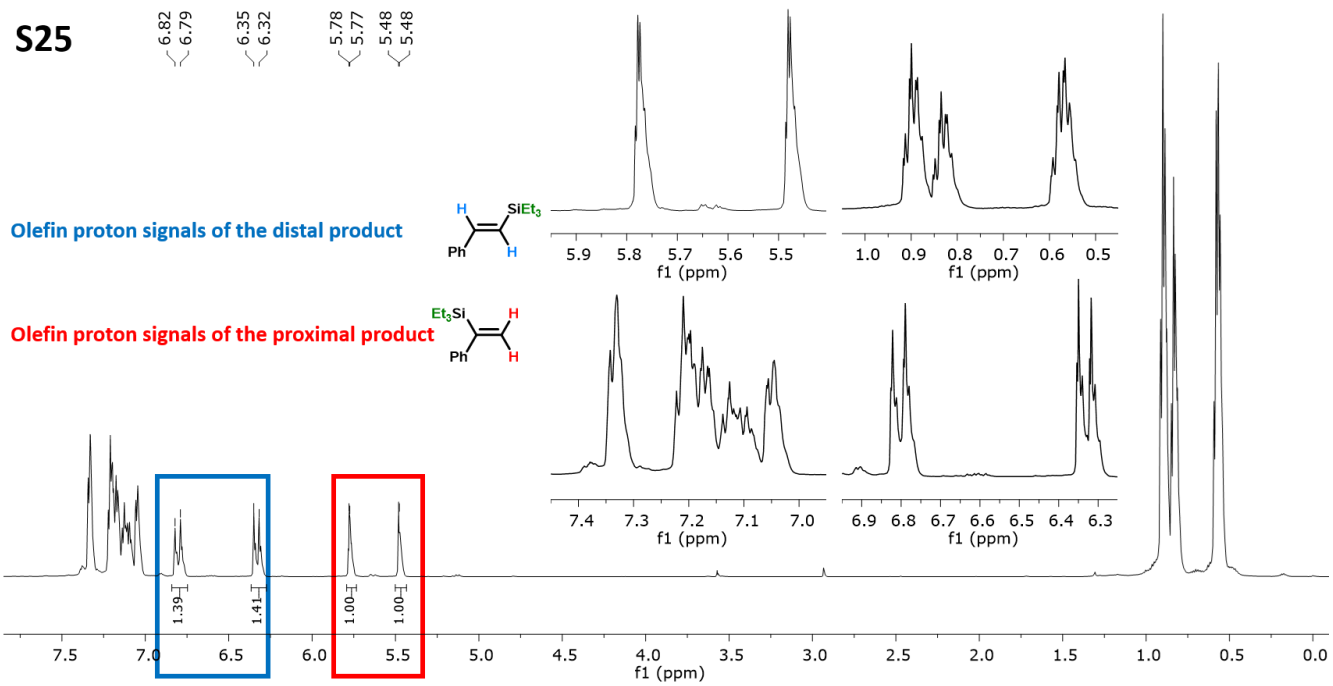

Figure S25 ^{1}H NMR spectrum (300.13 MHz, $CDCl_3$) with expanded sections of the hydrosilylation product from sample S25. The conversion was 99% and the molar distal/proximal ratio 1.4.

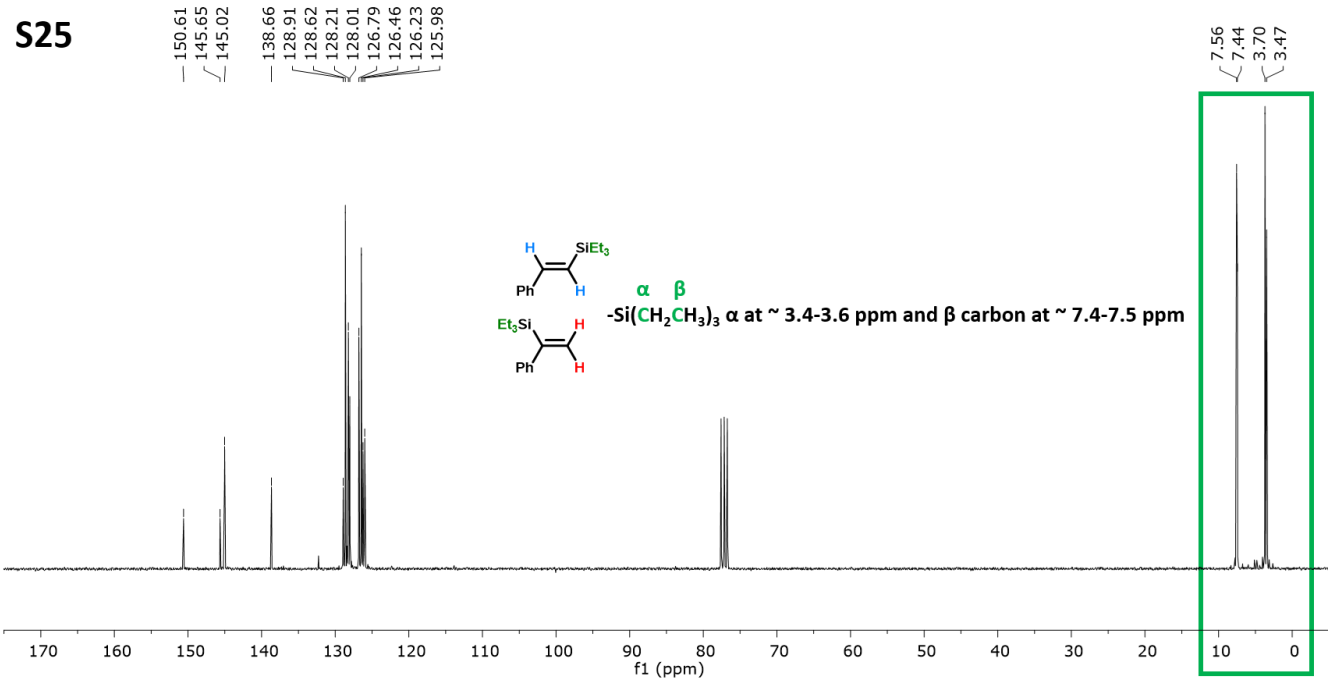

Figure S26 ^{13}C NMR spectrum (75.475 MHz, $CDCl_3$) of the hydrosilylation product from sample S25. Carbon α at ~3.4-3.6 ppm and carbon β at ~7.4-7.5 ppm. The two peaks each for α and β are due to the distal and proximal products.

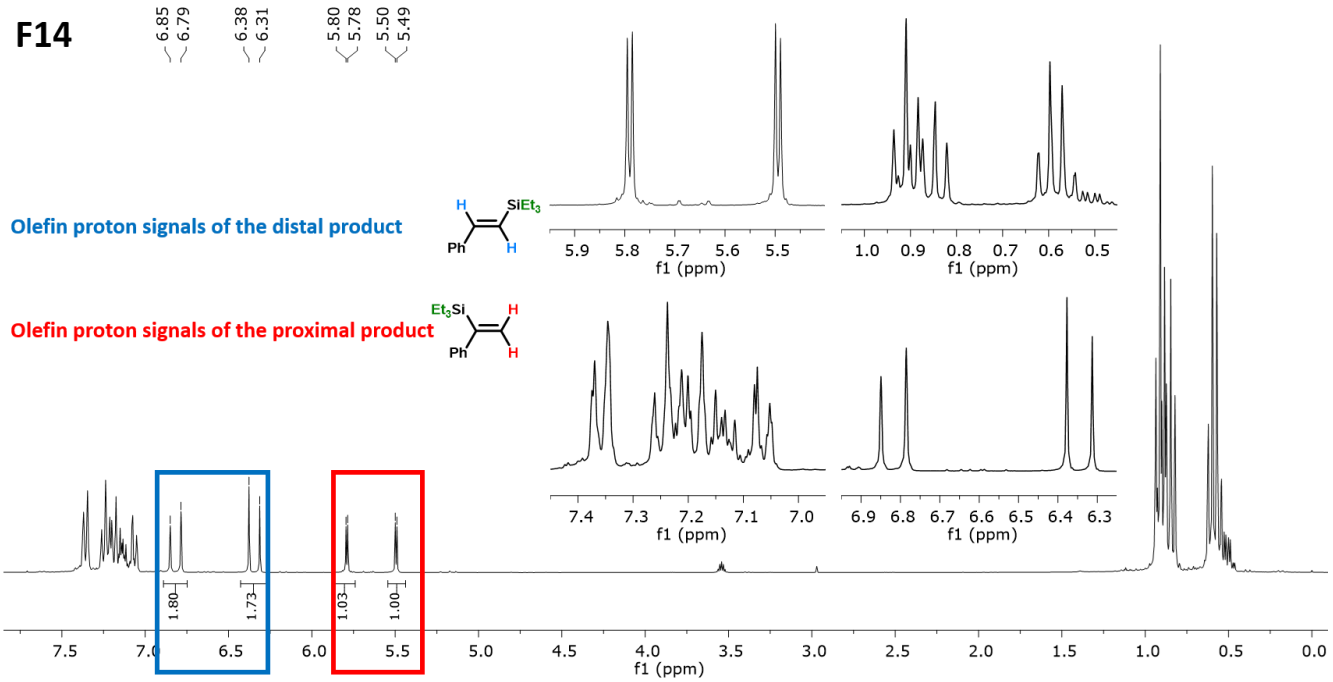

Figure S27 ^{1}H NMR spectrum (300.13 MHz, $CDCl_3$) with expanded sections of the hydrosilylation product from sample F14. The conversion was 98% and the molar distal/proximal ratio 1.7.

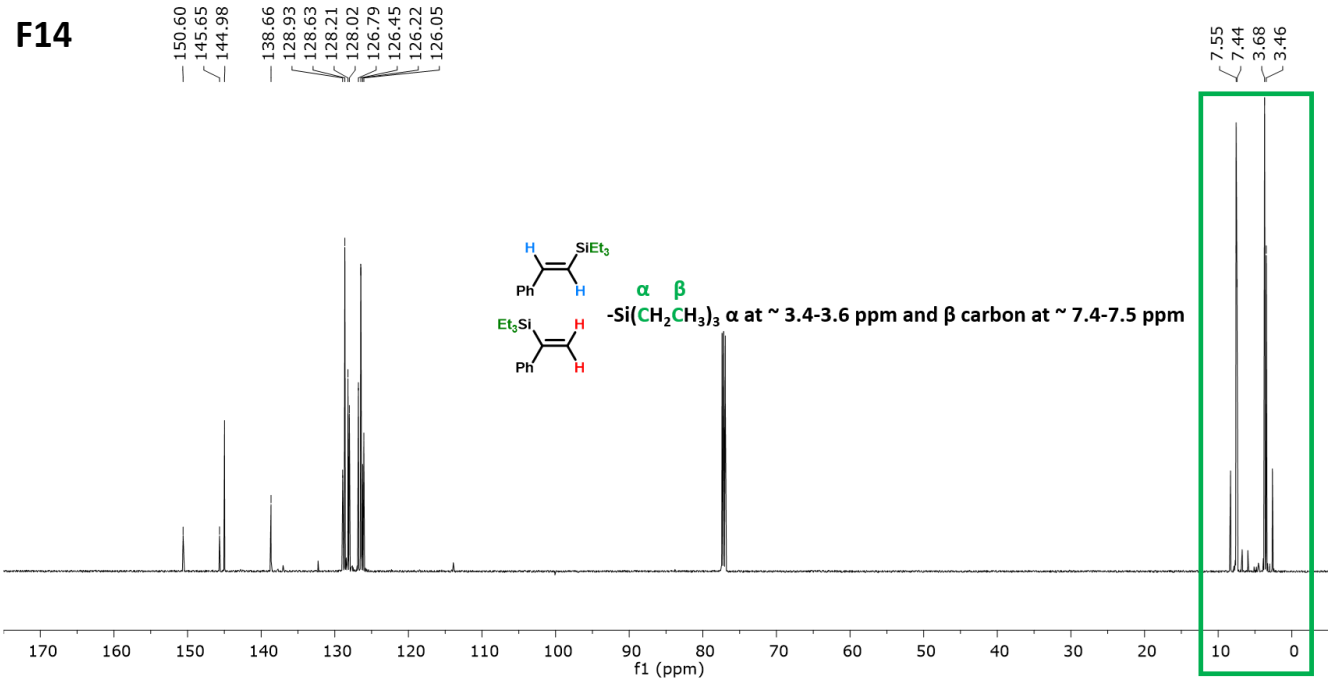

Figure S28 ^{13}C NMR spectrum (75.475 MHz, $CDCl_3$) of the hydrosilylation product from sample F14. Carbon α at ~3.4-3.6 ppm and carbon β at ~7.4-7.5 ppm. The two peaks each for α and β are due to the distal and proximal products.

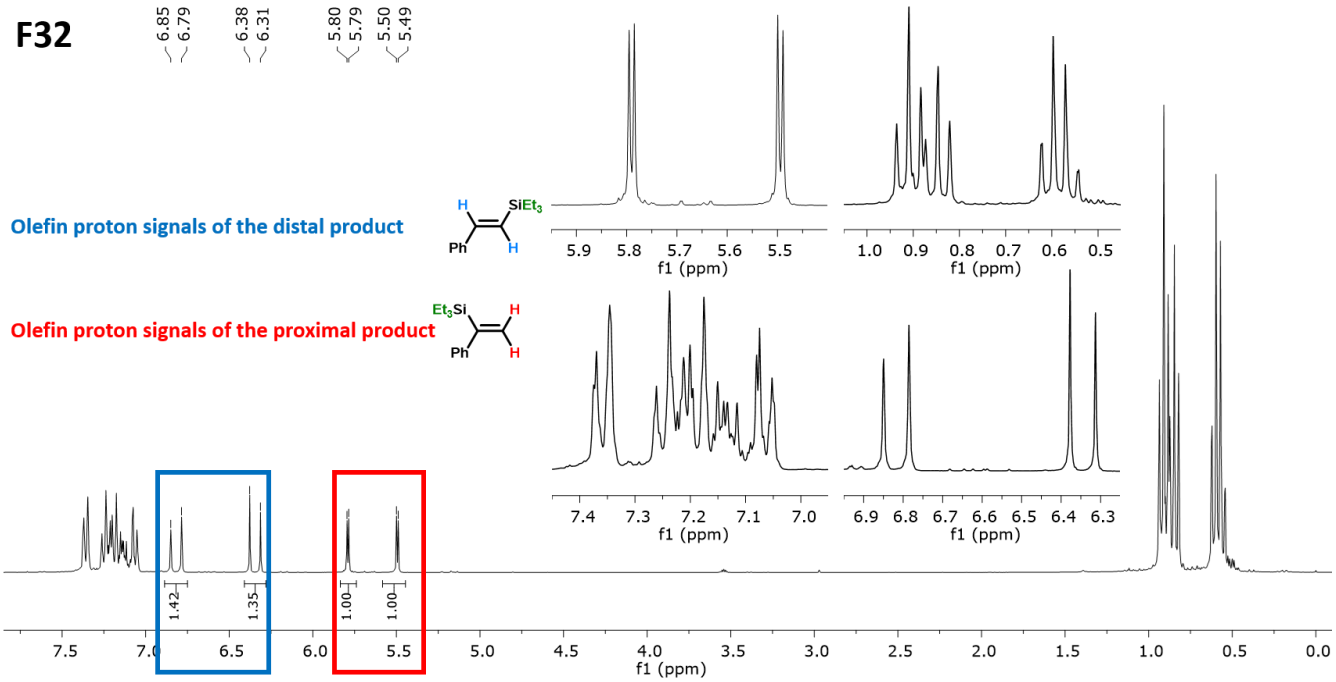

Figure S29 ^{1}H NMR spectrum (300.13 MHz, $CDCl_3$) with expanded sections of the hydrosilylation product from sample F32. The conversion and the distal/proximal ration obtained were 99% and 1.4, respectively.

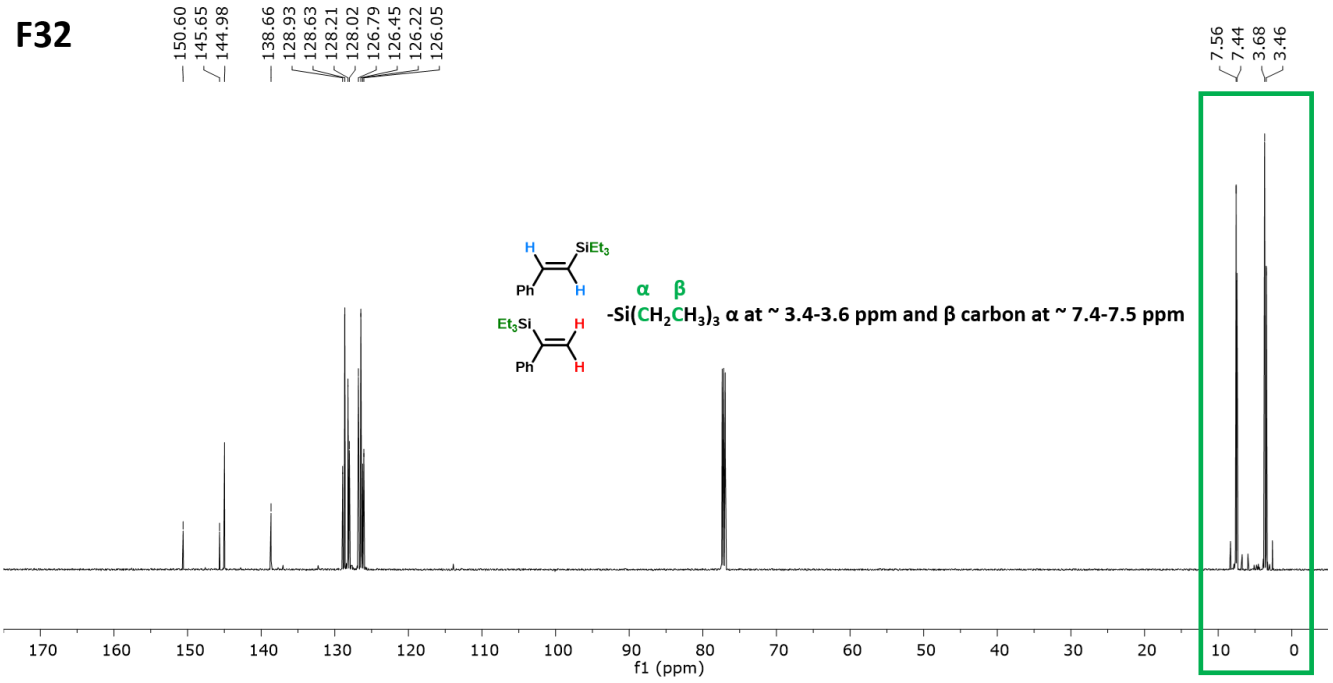

Figure S30 ^{13}C NMR spectrum (75.475 MHz, $CDCl_3$) of the hydrosilylation product from sample F32. Carbon α at ~3.4-3.6 ppm and carbon β at ~7.4-7.5 ppm. The two peaks each for α and β are due to the distal and proximal products.

S10 Gas chromatography (GC) analysis

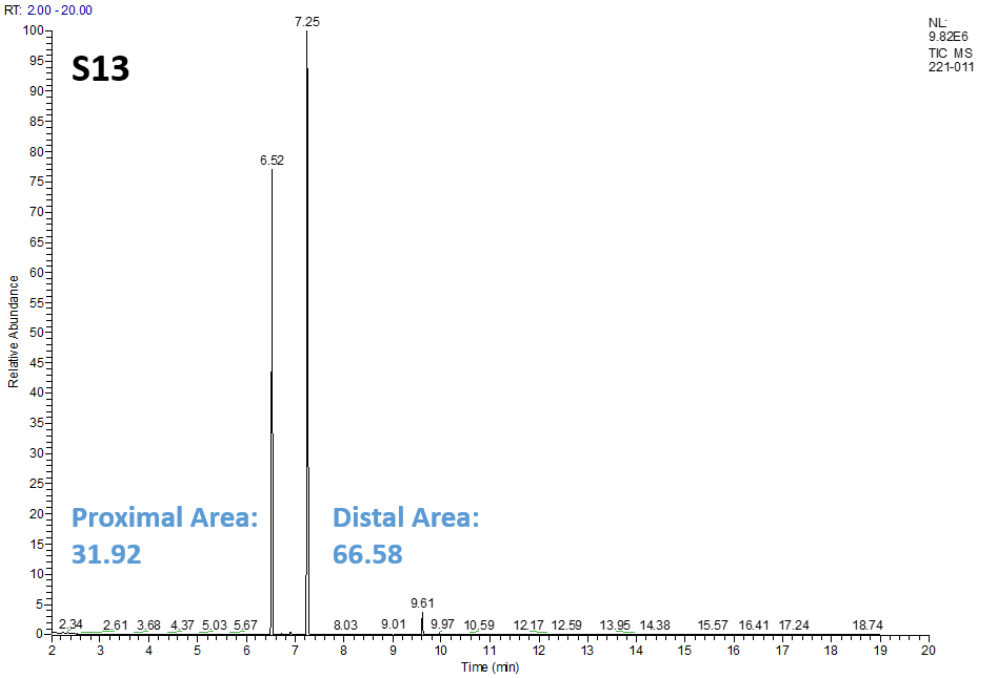

Figure S31 Gas chromatogram of the hydrosilylation product from sample S13. The molar distal/proximal ratio was 2.1.

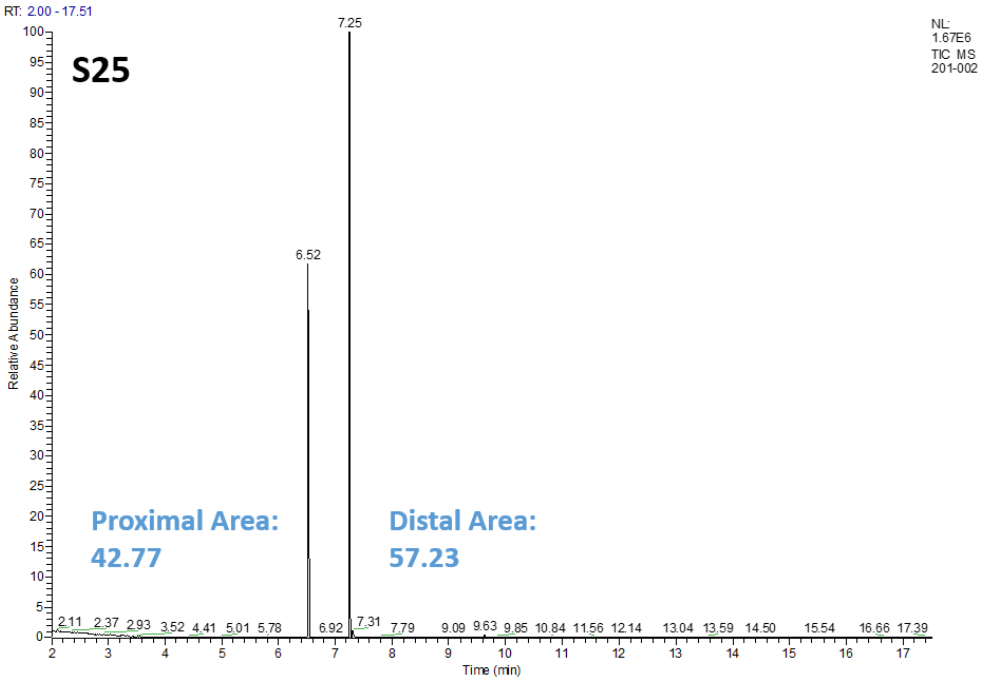

Figure S32 Gas chromatogram of the hydrosilylation product from sample S25. The molar distal/proximal ratio was 1.3.

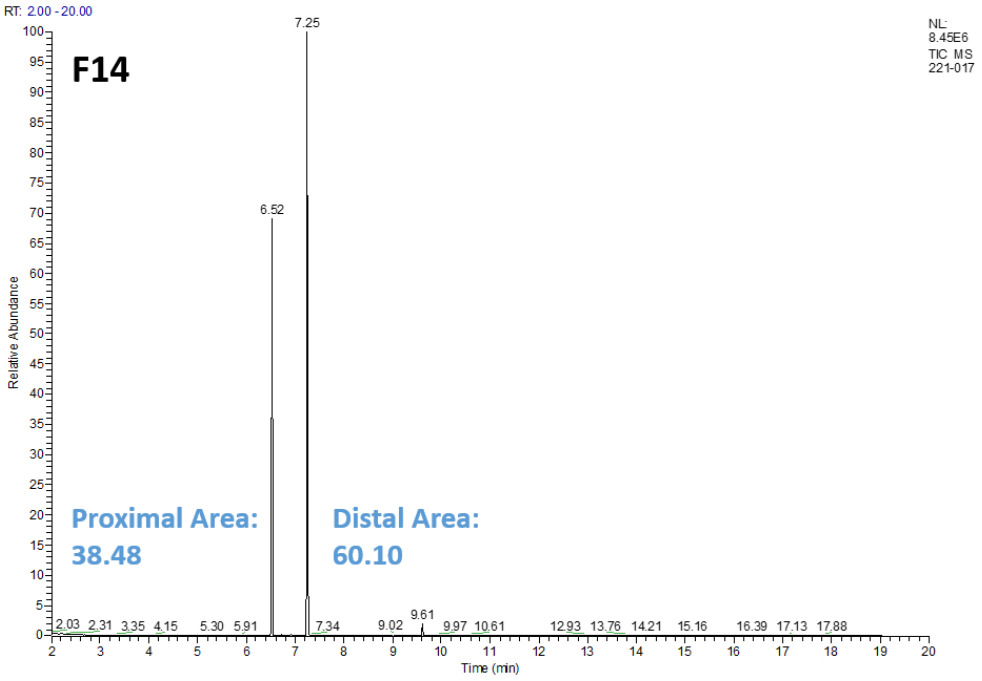

Figure S33 Gas chromatogram of the hydrosilylation product from sample F14. The molar distal/proximal ratio was 1.6.

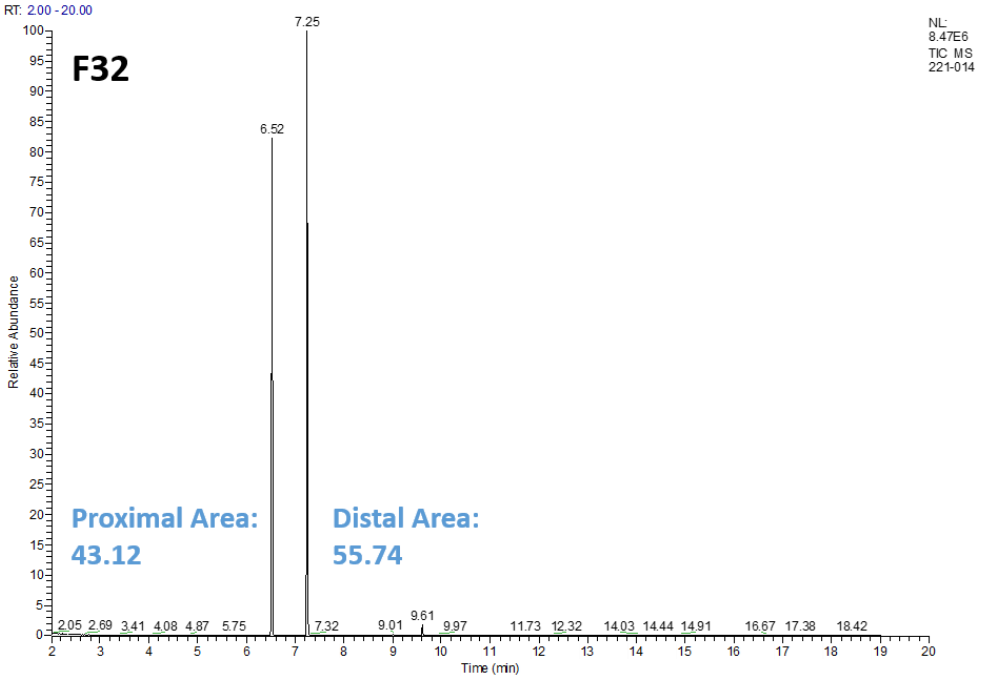

Figure S34 Gas chromatogram of the hydrosilylation product from sample F32. The molar distal/proximal ratio was 1.3.

References

42 Troegel, D.; Stohrer, J. Recent advances and actual challenges in late transition metal catalyzed hydrosilylation of olefins from an industrial point of view. *Coord. Chem. Rev.* **2011**, *255*, 1440–1459. https://doi.org/10.1016/j.ccr.2010.12.025.

50 Chalk, A. J.; Harrod, J. F. Homogeneous Catalysis. II. The Mechanism of the Hydrosilation of Olefins Catalyzed by Group VIII Metal Complexes 1. *J. Am. Chem. Soc.* **1965**, *87*, 16–21. https://doi.org/10.1021/ja01079a004.

63 Chauhan, M.; Hauck, B. J.; Keller, L. P.; Boudjouk, P. Hydrosilylation of alkynes catalyzed by platinum on carbon. *J. Organomet. Chem.* **2002**, *645*, 1–13. https://doi.org/10.1016/S0022-328X(01)01103-2.
70 Max, J.-J.; Chapados, C. Glucose and fructose hydrates in aqueous solution by IR spectroscopy. *J. Phys. Chem. A* **2007**, *111*, 2679–2689. https://doi.org/10.1021/jp066882r.
71 Yong, L.; Kirleis, K.; Butenschön, H. Stereodivergent Formation of Alkenylsilanes:syn oranti Hydrosilylation of Alkynes Catalyzed by a Cyclopentadienylcobalt(I) Chelate Bearing a Pendant Phosphane Tether. *Adv. Synth. Catal.* **2006**, *348*, 833–836. https://doi.org/10.1002/adsc.200606028.